https://doi.org/10.20965/ijat.2021.p0182

Paper:

Localization System for Indoor Mobile Robot Using Large Square-Shaped Reflective Marker

Hiroaki Seki[∗,†], **Ken Kawai**[∗∗], **and Masatoshi Hikizu**[∗∗∗]

[∗]Faculty of Frontier Engineering, Kanazawa University
Kakuma-machi, Kanazawa, Ishikawa 920-1192, Japan
[†]Corresponding author, E-mail: hseki@se.kanazawa-u.ac.jp
[∗∗]Graduate School of Natural Science and Technology, Kanazawa University, Kanazawa, Japan
[∗∗∗]Faculty of Production Systems Engineering and Sciences, Komatsu University, Komatsu, Japan
[Received August 18, 2020; accepted January 26, 2021]

A localization system using reflective markers and a fisheye camera with blinking infrared lights is useful and safe for mobile robot navigation in an environment with coexisting humans and robots; however, it has the problems of low robustness and a small measurable range for marker detection. A large, square-shaped reflective marker, with solid and dotted edges, is proposed for more reliable localization of indoor mobile robots. It can be easily detected using Hough transform and is robust for occlusion. The coordinates of the four corners of the square-shaped marker determine the robot's localization. Infrared lighting with a new LED arrangement is designed for a wide measurable range via brightness simulation, including the effect of observation and reflection angles. A prototype system was developed, enabling the 2D position and orientation to be detected with an accuracy of 60 mm and 3°, respectively, within a 4 m^2 area.

Keywords: localization, mobile robot, retro-reflective marker, infrared LED, Hough transform

1. Introduction

Recently, service robots have been employed in proximity to humans [1]. Reliably detecting the position of these robots is a key technology for their general movement. The localization system should also be harmless and unobstructive to humans. Intelligent visual 3D recognition of natural landmarks, as exhibited by humans, is the most ideal method and many researchers have utilized novel algorithms, in combination with cameras or laser range finders, to achieve this [2–5]; however, they are not sufficiently reliable for use in various environments. Methods using artificial landmarks are effective in easily and reliably locating a robot's position. Several types of localization systems have been developed. Visible markers with special patterns and colors are often used for robot localization as they can be installed very easily [6–9]. However, they can be affected by lighting and occlusion. The system utilizing a scanning laser light [10, 11] is expensive and lacks eye-safety for humans. Active beacon systems using ultrasound [12, 13], infrared light [14, 15], etc., exhibit highly reliable and accurate localization; however, their beacons require a power supply and implementation tends to be complicated. Although RF waves are frequently proposed for localization [16, 17], they do not allow sufficient positional accuracy. From the above, it can be said that there are few localization systems suitable for environments with coexisting humans and robots.

We have already proposed a localization system using reflective markers for indoor mobile robots [18]; i.e., a reliable, safe, and inexpensive marker-based localization system that uses a camera. A similar system using reflective markers has also been developed in [19, 20]. However, they have some drawbacks. For example, the system in [20] uses 16 cm or 28 cm square reflective AR markers, with 1 cm or 2 cm square grid patterns, that are attached to the ceiling at intervals of several tens of centimeters. These markers are small and their recognition is slightly complicated. This sometimes causes detection failure or occlusion by humans/furniture in a room. Another drawback is that its measurable range is limited because the brightness of the reflective markers in the camera image decreases with distance from the robot. A small measurable range requires many markers with complicated shapes for recognition, as in the above example, which is not effective.

Therefore, this paper proposes an improved localization system using a new reflective marker, comprising large and simple shapes, and infrared lighting with a new arrangement for a wide measurable range.

2. Localization System Using Reflective Marker

The proposed system is shown in **Fig. 1**. Retro-reflective tape, which is commercially used for safety goods, is utilized as a marker for detecting the robot's position. It has many micro-prism structures on the surface, and these reflect light to its source, irrespective of the incidence direction. Reflective markers on the ceiling are not obstructive to humans because their color can be matched

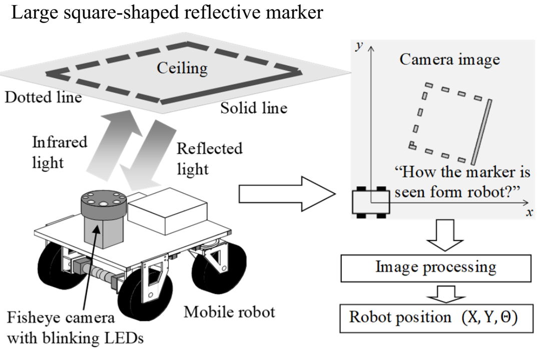

Fig. 1. Proposed localization system using reflective marker.

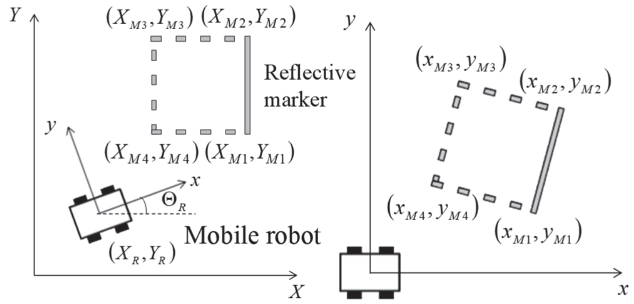

(a) Known marker position on the base coordinate system

(b) Detected marker position on the robot coordinate system

Fig. 2. Geometrical relation between camera image and robot's position.

to the ceiling, and they reflect light toward its source, even if the lights are visible. They are also inexpensive and easily installed in existing buildings.

We then attached reflective tape in a large square shape at a known location on an indoor ceiling. When the camera on a mobile robot captures an image of the ceiling, the view of this reflective marker is changed according to the robot's position and orientation. Thus, the position and orientation of the robot can be estimated by the marker's position and orientation in the image. To detect the marker's orientation, the marker should be anisotropic. Thus, one side of the square marker was a solid line and the other sides were dotted lines. This large, square-shaped marker is robust for occlusion. Four corners of this marker in the camera image are used to calculate the robot's position. They can be detected even when sides or corners of the square marker are partially hidden by humans/furniture. Details are mentioned later.

Some improvements are made for a wider detectable range and easier detection of reflective markers. A fisheye lens is mounted on the camera to capture the marker over a wide range. Infrared LEDs were also attached around the camera lens. When the LEDs are turned on, their infrared light is reflected toward the camera via reflective markers, which can capture a very bright image of the marker. Although infrared light is invisible to humans, the camera's image sensor is infrared-sensitive. Surrounding objects scatter the LED light and hence the image brightness does not significantly change. If the LEDs blink on/off, the subtracted image of the camera synchronizes with the blinking LED and can be utilized to eliminate the background images surrounding the reflective markers. If the diaphragm of the camera is adjusted for image brightness in ambient lighting to avoid saturation, the increased brightness of the reflective markers via the blinking LED can be captured. This LED blinking is controlled by the camera shutter signal. Since the subtracted image is not significantly affected by lighting and predominantly contains the marker's image, image processing for marker detection is easy and robust. The subtracted image is not perfect as the marker image and the movement image of humans due to the difference in image acquisition time remains. Therefore, we need to apply some image processing to isolate the marker.

3. Principle of Localization

At least two known positions in the reflective markers are necessary to determine the 2D position of a robot as it moves on a flat floor. However, considering higher reliability by redundancy, four corner positions of a large square marker are used to estimate the 2D position and orientation of the robot (X_R, Y_R, Θ_R) on the base coordinate system, as shown in **Fig. 2**.

Four corner positions (X_{Mi}, Y_{Mi}) $(i = 1,2,3,4)$ on the base coordinate system are known in advance. When a large, square-shaped reflective marker is detected in the visual field of a robot, four corner positions are obtained as (x'_{Mi}, y'_{Mi}) in the image. A fisheye lens is used and hence these coordinates are converted to (x_{Mi}, y_{Mi}) in the robot's coordinate system by:

$$\begin{bmatrix} x_{Mi} \\ y_{Mi} \end{bmatrix} = \frac{s}{s'} \begin{bmatrix} x'_{Mi} \\ y'_{Mi} \end{bmatrix}, \quad s = Z \tan\theta, \quad \ldots\ldots \quad (1)$$

$$s' = \sqrt{x'^2_{Mi} + y'^2_{Mi}} = f_\theta\left(\frac{s'C}{F}\right), \quad \ldots\ldots\ldots \quad (2)$$

where Z is the height of the ceiling from the camera, θ is the incident angle to the fisheye lens, F is the focal distance, C is the pixel size of the image sensor, and $f_\theta(\ )$ is the function of lens projection. The coordinate transformation of the marker position between the base and robot coordinate system is given by the robot's position.

$$\begin{bmatrix} X_{Mi} \\ Y_{Mi} \end{bmatrix} = \begin{bmatrix} \cos\Theta_R & -\sin\Theta_R \\ \sin\Theta_R & \cos\Theta_R \end{bmatrix} \begin{bmatrix} x_{Mi} \\ y_{Mi} \end{bmatrix} + \begin{bmatrix} X_R \\ Y_R \end{bmatrix}. \quad (3)$$

These are eight equations that are redundant for calculating the position and orientation of the robot (X_R, Y_R, Θ_R) from the four corner positions (X_{Mi}, Y_{Mi}) $(i = 1,2,3,4)$ of a square marker, measured by the camera. Therefore, we apply the steepest descent method to solve these equations numerically. The target function is set as:

$$f_j = \frac{1}{4}\sum_{i=1}^{4}\left\{\left(X'_{Mij} - X_{Mi}\right)^2 + \left(Y'_{Mij} - Y_{Mi}\right)^2\right\}, \quad (4)$$

where (X_{Mi}, Y_{Mi}) is the known location of four corners of a marker and (X'_{Mij}, Y'_{Mij}) is the corners' location calculated by Eq. (3), when the robot's position $(X_{Rj}, Y_{Rj}, \Theta_{Rj})$ is assumed. If the calculated robot's position approaches the true value, this target function tends to zero. The steepest descent method finds the direction in which the target function decreases most quickly and converges to the robot's position, as follows.

$$\begin{cases} X_{R(j+1)} = X_{Rj} - k_1 \dfrac{\partial f_j}{\partial X_R}, \\ Y_{R(j+1)} = Y_{Rj} - k_1 \dfrac{\partial f_j}{\partial Y_R}, \end{cases} \quad \dots\dots\dots \quad (5)$$

$$\Theta_{R(j+1)} = \Theta_{Rj} - k_2 \frac{\partial f_j}{\partial \Theta_R}, \quad \dots\dots\dots \quad (6)$$

where k_1, k_2 are coefficients for convergence, and are determined by trial-and-error for smooth and rapid convergence of the robot's position. Because the measured corner positions of a marker include some errors, this calculation is repeated until:

$$\left| f_{j+1} - f_j \right| < \delta_1 \quad \text{and} \quad f_j < \delta_2, \quad \dots\dots\dots \quad (7)$$

where δ_1, δ_2 are certain thresholds, related to the accuracy of the converged robot's position. Generally, the steepest descent method has the problem of a local minimum. However, the target function of this method only evaluates the position gaps about four corners of a square shape. This function is very simple and hence is considered to not have a significant local minimum.

In addition, we can set an arbitrary position as an initial value; however, setting the last robot's position can speed up convergence of the calculation.

4. Lighting Simulation and Prototype System

We created a prototype system, as shown in **Fig. 3**, based on the above concept. The specifications of each part is listed in **Table 1**. A large square-shaped reflective marker is made by attaching reflective tapes on the ceiling. For example, the length of a side is 2 m. We used a camera with a relatively strong sensitivity to near-infrared light. The projection function of the fisheye lens was calibrated by measuring the known locations.

The problem is the configuration and directivity of infrared LEDs for lighting. They determine the brightness of the reflective marker in the camera image, i.e., the detectable range of the reflective marker. If all LEDs are installed upward, the marker image becomes dimmer as the distance from the camera increases. Therefore, we evaluated the LED arrangement using the brightness simulation model shown in **Fig. 4**.

The distribution of the marker brightness on the ceiling is given by

$$I(x,y) = I_D(r)\, I_L(\theta)\, I_O(\alpha,\gamma), \quad \dots\dots\dots \quad (8)$$

where $I_D(r)$ is the attenuation by the distance r between the LED (camera) and the marker, $I_L(\theta)$ is the directivity of the LED, and $I_O(\alpha,\gamma)$ is the characteristic of the reflective marker by the observation angle α and reflection angle γ. $I_D(r)$ and $I_L(\theta)$ can be easily obtained by preliminary experiments or product catalogs and are expressed using approximation curves. $I_O(\alpha,\gamma)$ is nonlinear and not independent. Although the observation angle α is small, normally less than 1°, it strongly affects marker bright-

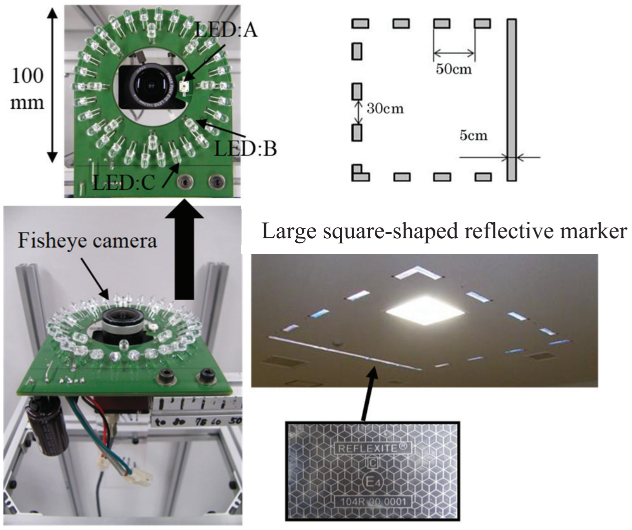

Fig. 3. Fisheye camera with LEDs and reflective marker on ceiling.

Table 1. Specifications of the developed localization system.

Unit	Model	Maker	Specifications
IEEE1394 camera	F-131 B NIR	Marlin	2/3 inch CMOS, 8 bit grey scale, 1280 × 1024 pixels
Fisheye lens	FI-23	FIT	Equisolid angle projection, Focus 2.3 mm, Covering angle 160°, Dia. 28 mm
Main infrared LED: A	SFH 4235	OSRAM	Peak 860 nm, 3.4 W, 320 mW/sr, Half angle ±60°
Sub infrared LED: B	TSHG 6410	VISHAY	Peak 850 nm, 180 mW, 900 mW/sr, Half angle ±18°
Sub infrared LED: C	SFH 4550	OSRAM	Peak 860 nm, 180 mW, 7000 mW/sr, Half angle ±3°
Reflective marking tape	JV 104E	Reflexite	Prism type, Width 50 mm

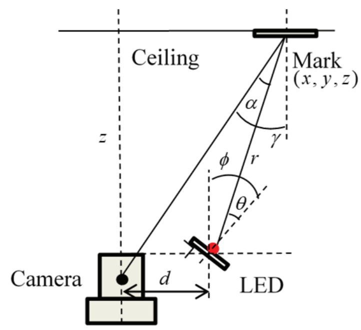

Fig. 4. Simulation model of marker brightness for LED arrangement.

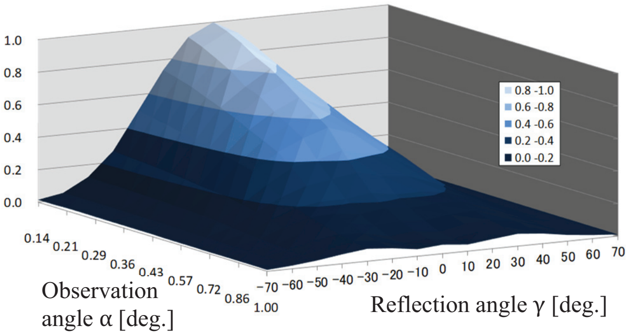

Fig. 5. Measured characteristic of marker brightness $I_O(\alpha,\gamma)$ by observation and reflection angle.

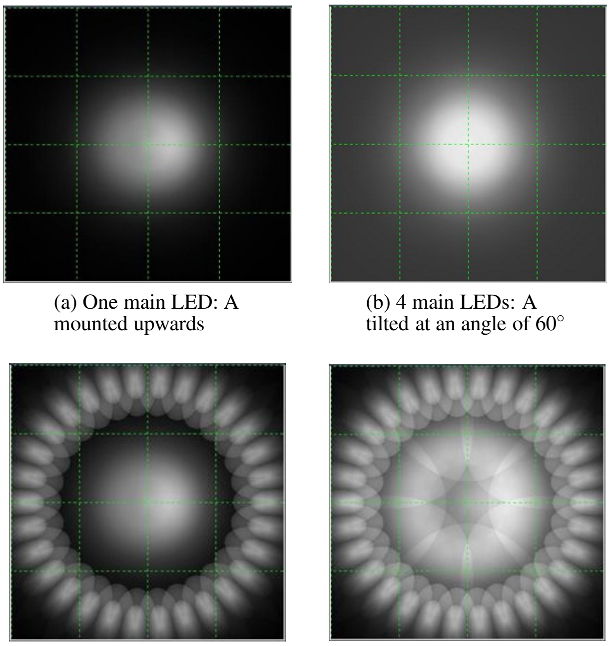

(a) One main LED: A mounted upwards

(b) 4 main LEDs: A tilted at an angle of 60°

(c) 1 main LED: A 0°, +30 sub LEDs: C 61°

(d) 1 main LED: A 0°, +8 sub LEDs: B 56°, +30 sub LEDs: C 61°

Fig. 6. Simulation results for marker brightness distribution on ceiling.

ness due to the property of retro-reflection. This characteristic was measured by placing the marker in front of the camera and changing the tilt angle of the marker and distance between the LED and camera. The result is shown in **Fig. 5** and is stored in a table for simulation.

Several brightness simulation results using Eq. (8) are shown in **Fig. 6**. The area of the marker for the simulation is 8 m square. The height of the ceiling from the camera is 2 m. **Fig. 6(a)** shows one main LED (type A) with a large output and wide directivity, mounted upward at a distance of 20 mm from the center of the camera lens, and **Fig. 6(b)** shows four main LEDs at a distance of 20 mm around the camera, tilted at an angle of 60°. We found that tilting LEDs with a wide directivity had little effect on increasing the brightness in the far area. After including LEDs with narrow directivity and repeatedly simulating combinations and arrangements of several LEDs (**Fig. 6(c)** for example), we finally obtained the reasonable result shown in **Fig. 6(d)**. In this case, three types of LEDs (**Table 1**) were used and their mounting angles changed. One main LED (type A) is mounted upwards at a distance of 20 mm from the camera. Eight sub LEDs (type B) and 30 sub-LEDs (type C) with narrow directivity are added at a tilt angle of approximately 60° and a distance of 36 mm and 45 mm, respectively, around the camera. Tilted LEDs with narrow directivity are effective for brightening the far area, although a small lack of uniformity is seen.

5. Detection of Reflective Marker

Marker detection is the key to reliable marker-based localization. In our proposed system, the 2D position of a robot can be estimated by the calculation previously mentioned, whereby four corners of a reflective marker in a large square can be captured.

Only reflective markers can be easily recognized by the following image processing, even if the image includes moving persons, lamps, furniture, etc. **Fig. 7** shows this process for the ceiling image of a room.

i. Image distortion by the fisheye lens is previously corrected for by applying Eqs. (1) and (2) to the lens projection for each camera image.

ii. A camera image is captured when the infrared LEDs around the camera is turned on. We can obtain a very bright image of the reflective marker.

iii. In the next moment, a camera image is captured when the LEDs are turned off; the reflective marker can scarcely be seen in the image.

iv. Most of the background images can be eliminated by the subtraction of the above two images when the LEDs are turned on/off because the brightness of the background is not changed significantly by the LED light. However, this is not perfect. Some objects and noise were left in the image. In particular, objects near the LEDs remain because they strongly reflect the LED light.

v. Binarization is applied to remove small noises.

vi. After erosion and dilation are applied to the image, in this order, the image of the reflective marker disappears because the line image has a narrow width.

vii. We subtracted the previous image without the marker from the binary image with a marker. A negative value in each pixel is regarded as zero in this process. Then, any large noise is removed, leaving almost only the marker image.

viii. Four lines of the square marker are detected by the Hough transform and these four lines lead to positions of the four corners for estimating the robot's position.

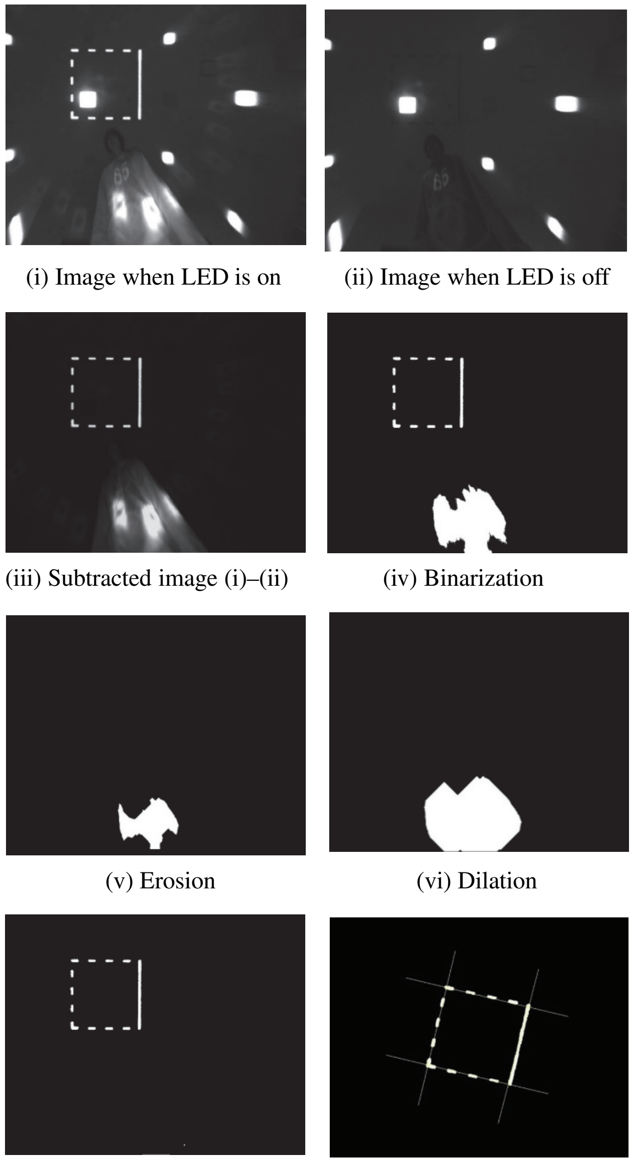

(i) Image when LED is on (ii) Image when LED is off

(iii) Subtracted image (i)–(ii) (iv) Binarization

(v) Erosion (vi) Dilation

(vii) Subtracted image (iv)–(vi) (viii) Line detection by Hough transform

Fig. 7. Image processing to detect large square-shaped reflective marker.

The extraction of four lines of a square marker in the camera image is discussed. The Hough transform is applied, as shown in **Fig. 8**, as it is robust against missing lines in the image due to occlusion or image processing failure. The line in the image is expressed by:

$$\rho = x\cos\theta + y\sin\theta, \qquad (9)$$

where ρ is the distance from the origin and θ is the inclination angle of a line. Pixels (x,y) in the final binary image detected by the previous method are voted on the space of ρ and θ. Because the square marker has four lines, the four local maxima are found in the voting results of ρ and θ. Parallel lines among them have the same angle θ, and the angles θ of the vertical lines are different by 90°. The distance between parallel lines is known as the side length of the square marker, d. Therefore, four

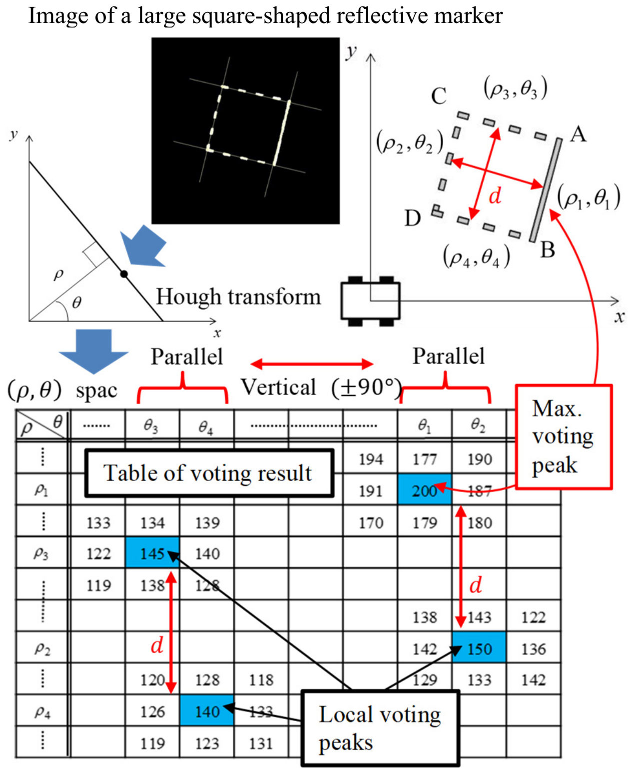

Fig. 8. Detection of four lines by Hough transform.

pairs of voting results of ρ and θ corresponding to four lines of a square marker can be discriminated by the above features, as follows.

i. A square marker comprises one solid line and three dotted lines. The maximum voting point (ρ_1,θ_1) is assigned as the parameter of one solid line because the pixels of a solid line are more than those of a dotted line.

ii. We try to find the local voting peak (ρ_2,θ_2) corresponding to the dotted line of the opposite side. Ideally, $\theta_2=\theta_1$, $|\rho_2-\rho_1|=d$ because the solid line and dotted line of its opposite side are parallel and are separated by the side length of a square marker d. Thus, we search the local voting peak near θ_1, at a distance of d from ρ_1.

iii. One (ρ_3,θ_3) of two dotted lines perpendicular to the solid line (ρ_1,θ_1) is found by searching the local voting peak near $\theta_1 \pm 90°$.

iv. Another (ρ_4,θ_4) of two dotted lines perpendicular to the solid line (ρ_1,θ_1) and parallel to the dotted line (ρ_3,θ_3) is detected by searching the local voting peak near $\theta_1 \pm 90°$ (or θ_3) and at a distance of d from ρ_3.

v. Four lines (ρ_n,θ_n), $n=1,2,3,4$, expressed by Eq. (9), obtain the coordinates of the four corners of the square marker.

vi. At this time, there are two possible configurations of the two lines (ρ_3,θ_3), (ρ_4,θ_4). One is shown in the

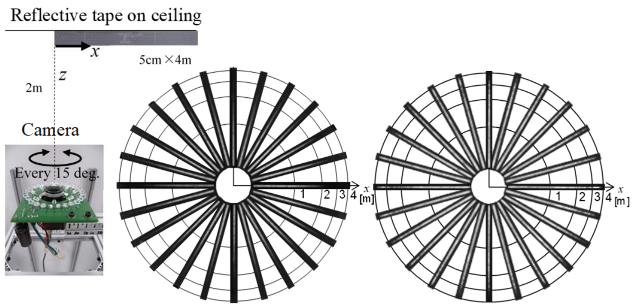

(a) Experiment (b) Case of **Fig. 6(a)** (c) Case of **Fig. 6(d)**

Fig. 9. Measured brightness of fisheye image of reflective tape.

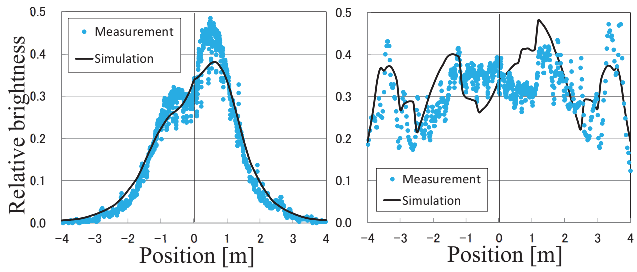

(a) Case of **Fig. 6(a)** (b) Case of **Fig. 6(d)**

Fig. 10. Example of measured brightness distribution along one line.

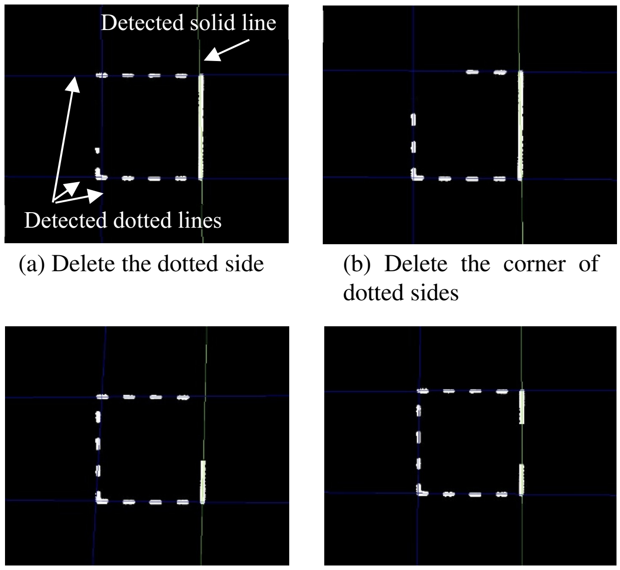

(a) Delete the dotted side (b) Delete the corner of dotted sides

(c) Delete the solid side (d) Delete the middle part of the solid side

Fig. 11. Limit of marker detection against occlusion.

upper-right figure of **Fig. 8**, and the order of the corners is ABDC (clockwise). The two lines are reversed in another configuration, and the order of the corners becomes BACD. These can be determined by the sign of $\overrightarrow{AB} \times \overrightarrow{AC}$ and four corners can be assigned to the known corner positions (X_{Mi}, Y_{Mi}) $(i = 1,2,3,4)$ on the base coordinate system.

vii. Additionally, when the four voting peaks with votes more than a certain threshold are not found, it is regarded as a failure for reliable localization.

6. Experiments

6.1. Brightness of Reflective Marker Image

First, the performance of the infrared LED lighting was verified as it is key for a wide detectable range of the reflective marker. The actual brightness of the marker in the camera image was measured by attaching reflective tape, 5 cm wide and 4 m long, to a ceiling 2 m above the camera. The current of each LED was 150 mA, and the light-on and light-off times were 40 ms and 120 ms, respectively. The diaphragm of the camera was adjusted so that the image brightness did not exceed the maximum greyscale for each experiment. Marker images were captured by rotating the camera every 15° and their overlapped image is shown in **Fig. 9**. Examples of the detailed distribution of the measured brightness along one line (x-axis) are shown in **Fig. 10**. The profile of the brightness almost corresponds well with the simulation. It is seen that the proposed arrangement using three types of LEDs (**Fig. 6(d)**) can extend the bright area up to approximately 4 m.

6.2. Robustness of Marker Detection

Next, the robustness of the proposed detection method of a large square-shaped marker against occlusion was evaluated. The real image of the marker in **Fig. 7(vii)** was tested as an example. The image size is 1280 × 1024 pixels and, in the image, the side length of the square marker is approximately 200 pixels. We investigated whether the four sides of the square marker could be detected after deleting a part of the marker image. In the Hough transform, the threshold for voting peaks was set to 80 pixels. To search for parallel or vertical lines, the distance and angle errors were set to ±10% of the side length and ±10°, respectively. We gradually removed more of the marker.

Figure 11 shows the results of the detection limit against occlusion. Mark images are enlarged by a factor of almost two in the figure. It can be found that our proposed method can detect lines even when occlusion is approximately half of each side of the marker. Although a single occlusion was tested this time, the detection method works with multiple occlusions by the combinations of **Figs. 11(a)–(d)** as the voting peaks of the Hough transform are determined by the number of pixels on each side of the marker image.

We explain the detection limit in each case. When the image lacks part of the dotted lines, as shown in **Figs. 11(a)** and **(b)**, the detection limit depends on the threshold for voting peaks. The side missing a larger part of the dotted line can be detected by the smaller threshold; however, it is easily affected by noise. When the image

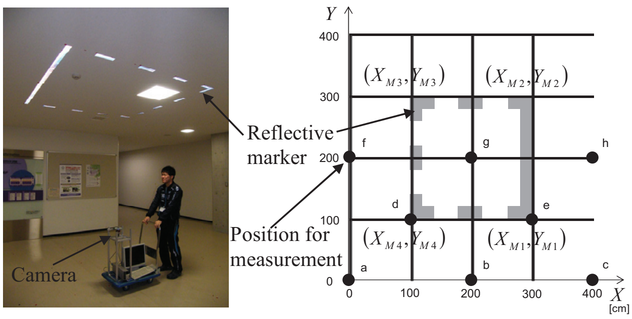

Markers are seen shining due to flash photography

Fig. 12. Set-up for localization experiments.

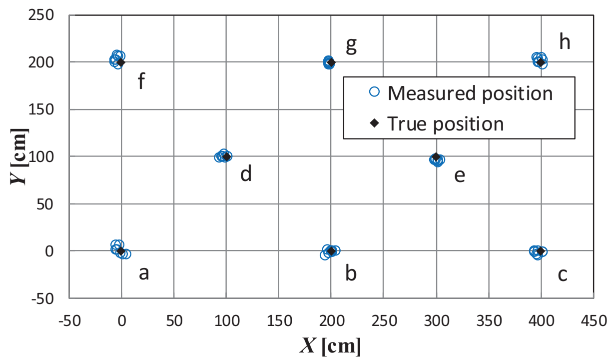

Fig. 13. Result of position measurement.

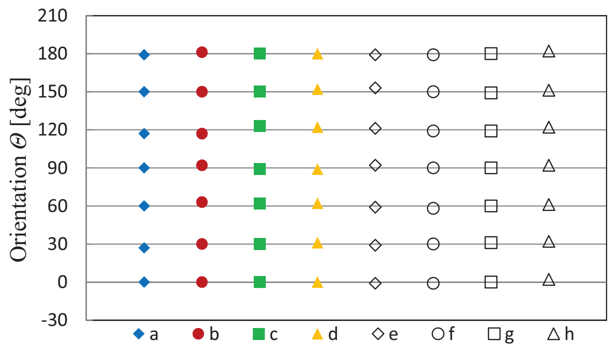

Fig. 14. Result of orientation measurement every 30° at locations "a–h."

lacks part of the solid line, as shown in **Figs. 11(c)** and **(d)**, the detection limit corresponds to the confusion of the dotted sides, i.e., the voting peak of the solid side with occlusion becomes smaller than that of the dotted side. This can be improved slightly by increasing the width of the solid side.

6.3. Position and Orientation Measurement

Localization experiments were conducted using the prototype system shown in **Fig. 12**. Reflective tapes 5 cm wide were attached to the ceiling at 2 m above the camera. The side length of the square marker was 2 m. A fluorescent lamp was also equipped near the marker and the local illuminance was approximately 100 lx. The current of each LED was 150 mA and the light-on and light-off times were 60 ms and 140 ms, respectively. The LEDs were synchronized by a camera with a framerate of 10 fps and an exposure time of 60 ms. Positions and orientations were measured at places "a–h" in **Fig. 12**. They cover half the area around the marker. Orientations were measured every 30° at each location by rotating the camera. These results are shown in **Figs. 13** and **14**. The measurement errors were less than 60 mm for position and 3.0° for orientation; this is acceptable for mobile robot localization. It was also shown that the square marker with a side length of 2 m on the ceiling 2 m above the camera enables a measurable area of 4 m square for localization.

The localization error is analyzed as follows: the main errors caused by the calibration error of the fisheye lens, tilting of the camera mount, and detection error of the four corners of the square marker. These directly affect the localization error because the known marker position on the base coordinate system and the detected marker position on the robot coordinate system are compared to estimate robot localization as shown in **Fig. 2**.

After calibrating the projection function of the fisheye lens, its error reached a maximum of 36 mm for the ceiling 2 m high, within 3 m (angle of view ±56°) from the point above the camera. Although this fisheye lens can obtain wide image of the ceiling within approximately 10 m from the camera, the calibration error at the position over 3 m becomes quite large. Tilting the camera mount increases the projection error. For example, a tilting angle of 0.1° causes a position error of 11 mm, 3 m from the camera, on a ceiling 2 m high. Detection of the four corners of the marker had an error of several pixels in the image because of the width of the marker. This corresponds to several tens of millimeters because the marker size of 2 m is approximately 200 pixels in the image. The errors of all four detected corners rarely shift in the same direction (translation or rotation) and hence, the localization error is less than their errors. If all four detected corners have an error of 50 mm in the same rotational direction, this causes an orientation error of 2.0° of the robot. The installation error of the marker on the ceiling can be less than several millimeters.

Considering the above errors, the measurement error from the localization experiments can be considered reasonable. The localization accuracy of the proposed method is the same as that of conventional systems using reflective markers. For example, the system in [19] achieved a position error of 19.4 mm and an orientation error of 1.64° in the range of 1 m^2, using an AR-like marker with a size of approximately 18 cm^2 on the ceiling 1.5 m above the camera. Another system in [20] obtained an average localization error of 150 mm and 8° when the robot moved 18 m, using approximately 80 AR markers in the range of 1.2 × 18 m on a 1.2 m high ceiling. Their markers are small and slightly complicated for robust detection. Comparing their systems, our proposed system will decrease the number of markers per unit area because the measurable range with reasonable localization error using one marker is wider.

7. Conclusions

A large, square-shaped reflective marker with solid and dotted lines has been proposed for more reliable localization of indoor mobile robots using a fisheye camera with blinking infrared lights. We have shown the detection method of this marker by image processing using the Hough transform and the calculation of the 2D robot's position and orientation from the four corners of the marker. In addition to the large size of this marker, easy detection via the Hough transform is robust for occlusion. To improve the measurable range, lighting with a new LED arrangement has been designed using a brightness simulation, including the effect of the observation and reflection angles of the marker. It was found that tilted LEDs with narrow directivity are effective for brightening the far area in the simulation. The lighting was a combination of three types of LEDs, with different directivities and mounting angles; we verified that it can, to some extent, uniformly brighten the marker on the ceiling several meters square. Finally, a prototype system was developed, which enabled the position and orientation to be detected every 0.1 s, with an accuracy of 60 mm and 3°, respectively, in a wide area of 4 m^2.

This system is sufficient for the navigation of a mobile robot in a room of several square meters. Square-shaped markers with different patterns are needed for a wider area; however, increasing the types of markers and detection robustness have a trade-off relation. Therefore, the combination of this large square-shaped marker and a small marker with an ID code, as an AR marker, is desirable and realistic for wider and global localization. In addition, we assume that the ceiling is flat and not tilted in our proposed method. If the ceiling is tilted, the image of a square-shaped marker becomes a quadrangle; our method has the possibility of application to this case by adjusting it to detect four lines of the marker via the Hough transform. This will be future work.

References:

[1] J. Tan, F. Duan, R. Kato, and T. Arai, "Man-Machine Interface for Human-Robot Collaborative Cellular Manufacturing System," Int. J. Automation Technol., Vol.3, No.6, pp. 760-767, 2009.

[2] L. B. Marinho et al., "Novel mobile robot localization approach based on topological maps using classification with reject option in omnidirectional images," Expert Systems with Applications, Vol.72, No.15, pp. 1-17, 2017.

[3] M. Nomatsu, Y. Suganuma, Y. Yui, and Y. Uchimura, "Development of an Autonomous Mobile Robot with Self-Localization and Searching Target in a Real Environment," J. Robot. Mechatron., Vol.27, No.4, pp. 356-364, 2015.

[4] K. Takahashi et al., "Performance Evaluation of Robot Localization Using 2D and 3D Point Clouds," J. Robot. Mechatron., Vol.29, No.5, pp. 928-934, 2017.

[5] V. Balaska, L. Bampis, M. Boudourides, and A. Gasteratos, "Unsupervised semantic clustering, and localization for mobile robotics tasks," Robotics and Autonomous Systems, Vol.131, 103567, 2020.

[6] K. Yoshida, "A Study on the On-Ground Access System Using Marker-Based Visual Imformation," J. Robot. Mechatron., Vol.15, No.1, pp. 84-95, 2003.

[7] H. Nakanishi and H. Hashimoto, "AR-Marker/IMU Hybrid Navigation System for Tether-Powered UAV," J. Robot. Mechatron., Vol.30, No.1, pp. 76-85, 2018.

[8] W. T. Huang, C. L. Tsai, and H. Y. Lin, "Mobile Robot Localization Using Ceiling Landmarks and Images Captured form an RGB-D camera," Proc. of the 2012 IEEE/ASME Int. Conf. on Advanced Intelligent Mechatronics, pp. 855-860, 2012.

[9] D. Nemec et al., "Precise localization of the mobile wheeled robot using sensor fusion of odometry, visual artificial landmarks, and inertial sensors," Robotics and Autonomous Systems, Vol.112, pp. 168-177, 2019.

[10] Z. Huang et al., "Accurate 3-D Position and Orientation Method for Indoor Mobile Robot Navigation Based on Photoelectric Scanning," IEEE Trans. on Instrumentation and Measurement, Vol.64, No.9, pp. 2518-2529, 2015.

[11] T. Tsuruta, K. Miura, and M. Miyaguchi, "Mobile robot for marking free access floors at construction sites," Automation in Construction, Vol.107, 102912, 2019.

[12] H. Seki et al., "Position System for Indoor Mobile Robot Using Active Ultrasonic Beacons," Proc. of the 3rd IFAC Symp. on Intelligent Autonomous Vehicles, pp. 681-686, 1998.

[13] K. Tabata, T. Iwai, S. Kudomi, Y. Endo, and Y. Nishida, "Precision Improvement of Position Measurement Using Two Ultrasonic Land Markers," J. Robot. Mechatron., Vol.26, No.2, pp. 245-252, 2014.

[14] K. Watanabe, Y. Yamada, and I. Nagai, "The Development of a 3D Position Measurement System for Indoor Aerial Robots," Proc. of the 14th Int. Conf. on Control, Automation and Systems, pp. 1185-1190, 2014.

[15] J. Wang and Y. Takahashi, "Indoor mobile robot self-localization based on low-cost light system with novel emitter arrangement," Robomech J., Vol.5, 17, doi: 10.1186/s40648-018-0114-x, 2018.

[16] S. Jia, J. Sheng, D. Chugo, and K. Takase, "Human Recognition Using RFID Technology and Stereo Vision," J. Robot. Mechatron., Vol.21, No.1, pp. 28-35, 2009.

[17] A. Ismail et al., "A Novel Automated Construction Method of Signal Fingerprint Database for Mobile Robot Wireless Positioning System," Int. J. Automation Technol., Vol.11, No.3, pp. 459-471, 2017.

[18] H. Seki et al., "Positioning System for Indoor Mobile Robots Using Reflective Marks and Fisheye Camera with Infrared LEDs," Proc. of the 5th Franco-Japanese and 3rd European-Asian Congress on Mechatronics, pp. 142-147, 2001.

[19] F. Zhou et al., "A high precision visual localization sensor and its working methodology for an indoor mobile robot," Frontiers of Information Technology and Electronic Engineering, Vol.17, pp. 365-374, 2016.

[20] Y. Nakazato, M. Kanbara, and N. Yokoya, "A Localization System Using Invisible Retro-reflective Markers," Proc. of the IAPR Conf. on Machine Vision Applications, pp. 140-143, 2005.

Name:
Hiroaki Seki

Affiliation:
Professor, Institute of Science and Engineering, Kanazawa University

Address:
Kakuma-machi, Kanazawa, Ishikawa 920-1192, Japan

Brief Biographical History:
1994- Research Associate, The University of Tokyo
1997- Kanazawa University

Main Works:
• "Development of assistive robotic arm for power line maintenance," Precision Engineering, Vol.67, pp. 69-76, 2021.
• "3-D Obstacle Detection Using Laser Range Finder with Polygonal Mirror for Powered Wheelchair," Int. J. Automation Technol., Vol.9, No.4, pp. 373-380, 2015.

Membership in Academic Societies:
• Japan Society of Mechanical Engineers (JSME)
• Japan Society for Precision Engineering (JSPE)
• Robotics Society of Japan (RSJ)

Name:
Ken Kawai

Affiliation:
Graduate Student, Graduate School of Natural Science and Technology, Kanazawa University

Address:
Kakuma-machi, Kanazawa, Ishikawa 920-1192, Japan

Brief Biographical History:
2012- Graduate School of Natural Science and Technology, Kanazawa University

Name:
Masatoshi Hikizu

Affiliation:
Associate Professor, Faculty of Production Systems Engineering and Science, Komatsu University

Address:
1-3 Nu, Shichou-machi, Komatsu, Ishikawa 923-8511, Japan

Brief Biographical History:
1995- Research Associate, Kanazawa University
2018- Komatsu University

Main Works:
• "Effects and Application of Current Feedback in Servo System with Current Limiter," Int. J. Automation Technol., Vo.11, No.1, pp. 104-111, 2017.
• "Motion Planning System for Bin Picking using 3-D Point Cloud," J. of Intelligent Control and Automation, Vol.7, No.3, pp. 73-83, 2016.

Membership in Academic Societies:
• Japan Society of Mechanical Engineers (JSME)
• Japan Society for Precision Engineering (JSPE)
• Robotics Society of Japan (RSJ)